Catalysis Today 166 (2011) 146–151

Contents lists available at ScienceDirect

Catalysis Today

journal homepage: www.elsevier.com/locate/cattod

Degradation of the herbicide 2,4-dichlorophenoxyacetic acid over $Au/TiO_2–CeO_2$ photocatalysts: Effect of the CeO_2 content on the photoactivity

C. Guzmán [a], G. del Ángel [a,*], R. Gómez [a], F. Galindo-Hernández [b], C. Ángeles-Chavez [c]

[a] Universidad Autónoma Metropolitana-Iztapalapa, Department of Chemistry, San Rafael Atlixco 186, A.P. 55-534, México, D.F. 09340, Mexico
[b] Universidad Nacional Autónoma de México (U.N.A.M.), A.P. 20-364,México City 01000, Mexico
[c] Instituto Mexicano del Petróleo, Eje Central Lázaro Cárdenas No. 152, México, D.F. C.P 07730, Mexico

ARTICLE INFO

Article history:
Available online 5 October 2010

Key words:
Gold photocatalysts
Titania–ceria photocatalysts: Titania–ceria energy band gap
2,4-D photodegradation

ABSTRACT

$Au/TiO_2–CeO_2$ photocatalysts were studied in the photodegradation of the 2,4-dichlorophenoxyacetic acid (2,4-D) in aqueous medium under UV light emission source. The $TiO_2–CeO_2$ supports (2.5–10 wt.% CeO_2) were prepared by the sol–gel method using titanium alkoxide and cerium nitrate as starting precursors. Gold nanoparticles were prepared by the deposition–precipitation method with urea and deposed on the supports to obtain $Au/TiO_2–CeO_2$ photocatalysts. The BET area increases as function of the CeO_2 content from 64 m^2/g for the bare TiO_2 solid to 71–137 m^2/g for the $TiO_2–CeO_2$ mixed oxides. TEM and HRTEM images showed Au nanoparticles ranking from 8.1 to 3.4 nm. Additionally well defined gold plasmon and a red shift in the E_g band gap energy (3.14–2.47 eV) was observed by UV–vis spectroscopy on the mixed oxides. For the photodegradation of 2,4-D it has been observed an important effect of cerium oxide in the photoactivity, it varies from 78 to 99% of 2,4-D conversion and from 61 to 88% of total organic carbon conversion for the Au/TiO_2 and $Au/TiO_2–CeO_2$ photocatalysts respectively. A synergetic effect where gold plays the role of electrons tramp and the cerium oxide the role of oxidizing agent is proposed.

1. Introduction

Due to health problems caused by the herbicide 2,4-dichlorophenoxyacetic acid (2,4-D) in people and animals, the 2,4-D was considered by EPA [1] as a recalcitrant pollutant. This pollutant can be found in wastewater from agricultural regions and its elimination has attracted the attention of researchers dedicated to the preparation of semiconductor materials with photocatalytic properties [2–6]. In this way new semiconductors materials with applications in the photodegradation of polluting compounds, organic compounds have been reported recently. By instance titania basis mixed oxides as $TiO_2–In_2O_3$ [3] and $TiO_2–CeO_2$ [7] had been reported as good photocatalysts for the degradation of the herbicide 2,4-D. Nevertheless, it has been found that gold nanoparticulated supported on TiO_2 greatly promotes the photoactivity [8–11] and important applications of gold in solar cells have been reported [12–14]. In this way, we decide to study the photocatalytic properties of the $Au/TiO_2–CeO_2$ solids, and with the objective to determine the main variables controlling the photoactivity in these materials, the photodegradation was studied as a function of the CeO_2 content. In the present study, we deposited gold onto $TiO_2–CeO_2$ to obtain $Au/TiO_2–CeO_2$ photocatalysts to degrade 2,4-D under UV light irradiation in an aqueous suspension.

In the present work due to its photoactivity properties the combination of $TiO_2–CeO_2$ supports and Au forming $Au/TiO_2–CeO_2$ photocatalyst is reported. The $TiO_2–CeO_2$ supports were prepared by sol–gel method at different contents of the cerium oxide (2.5–10 wt.%) and the gold nanoparticles (2.0 wt.%) were prepared by deposition–precipitation method with urea to obtain $Au/TiO_2–CeO_2$ photocatalysts. The characterization was done by nitrogen adsorption UV–vis diffusion reflectance spectroscopy (DRS), HAADF–STEM and the photocatalytic activity was tested in the the 2,4-D photodegradation under UV light emission.

2. Experimental

2.1. Photocatalysts preparation

The preparation of TiO_2 and titania–ceria $TiO_2–CeO_2$ supports was made as it has been reported elsewhere [15] in brief follows: the appropriate amount of $Ce(NO_3)_3·6H_2O$ (Strem Chemicals 99.9% Ce) was added to a vessel containing an ethanol/water solution (2:1 molar ratio) in order to obtain 0.0, 2.5, 5.0 and 10 wt.% CeO_2 in the doped titania. Then, 1 mol of titanium butoxide (Aldrich 97%) was added drop wise for 1 h. After gelling, the

* Corresponding author. Tel.: +52 55 58044668; fax: +52 55 58044666.
E-mail addresses: gdam@xanum.uam.mx, gloria.del.angel@hotmail.com (G. del Ángel).

0920-5861/$ – see front matter © 2010 Elsevier B.V. All rights reserved.
doi:10.1016/j.cattod.2010.09.009

sample was dried in air at 373 K over night and calcined at 773 K for 4 h. On the other hand, Au/TiO_2 and Au/TiO_2–CeO_2 solids were prepared by deposition–precipitation with urea [16]. To 5.0 g of support was added 125 mL of an aqueous 4.2×10^{-3} M solution of $HAuCl_4$ (Aldrich 49% Au) and urea (0.42 M). Afterwards, the suspension was centrifuged, washed, dried and calcined with air flow at 300 °C. After this treatment, gold is in the metallic state [17]. The nominal concentration of gold was 2.0 wt.%. The Au content of the materials was determined by inductively coupled argon plasma–atomic emission spectrometry (ICAP–AES). The elemental analysis, by ICAP–AES, showed gold contents on the catalysts around 2.0–2.1 wt.%. The photocatalysts were labeled as Au/TiO_2–CeO_2-*X* where *X* is the CeO_2 content.

2.2. Characterization

2.2.1. Adsorption measurements

The determination of the specific surface area was carried out in an automatic Quantachrome Autosorb 3B instrument. The Nitrogen adsorption isotherms were carried out at 77 K on outgassed samples overnight at 573 K. The specific surface areas were calculated from the desorption isotherms by using the BET equation, the BJH method was used to calculate the mean pore size distribution [18].

2.2.2. UV–vis absorption spectra

The UV–vis absorption spectra were obtained with a Varian Cary-III UV–vis spectrophotometer coupled with an integration sphere for diffuse reflectance studies. A sample of MgO with a 100% reflectance was used as a reference.

2.2.3. HAADF–STEM characterization

High angle annular dark field (HAADF) and scanning transmission electron microscopy (STEM) analysis of the samples was performed in a JEE-2200FS transmission electron microscope with an accelerating voltage of 200 kV. The microscope is equipped with a Schottky-type field emission gun and an ultra high resolution (UHR). Configuration (*Cs* = 0.5 mm; *Cc* = 1.1 mm; point to point resolution = 0.19 nm); and an in-column omega-type energy filter. The samples were ground, suspended in isopropanol at room temperature and dispersed with ultrasonic agitation; then, an aliquot of the solution was dropped on a 3 mm diameter holey copper grid.

The mean particle size (*ds*) of the Au particles was calculated by means of the following equation:

$$ds = \frac{\sum_{i=1}^{n} n_i d_i^3}{\sum_{i=1}^{n} n_i d_i^2}$$

where d_i is the diameter measured directly from the electron micrographs; and n_i is the number of particles having the diameter d_i.

2.2.4. Photocatalytic activity

Photodegradation experiments were carried out at room temperature (at 298 K) as follows: 125 mg of catalyst were added to a flask containing an aqueous solution (200 mL) with 17.6 ppm of 2,4-dichlorophenoxyacetic acid. The solution was fluxed with air (Air-Pump BOYU S-4000B, pressure: 0.012 MPa, Power: 9 W and output: 3.2 L/min) and maintained under stirring for 15 min in dark until reach the adsorption–desorption equilibrium, then it was irradiated in a closed box with an UV lamp Pen-Ray (UVP), which emits a radiation $\lambda = 254$ nm with a emission of 2000 $\mu W/cm^2$. The reaction rate was followed by taking samples every 15 min and then analyzed in a UV–vis spectrophotometer Varian, model Cary-III. The concentration of 2,4-diclorophenoxyacetic acid was calculated from the adsorption band at 282 nm, applying the Lambert–Beer equation.

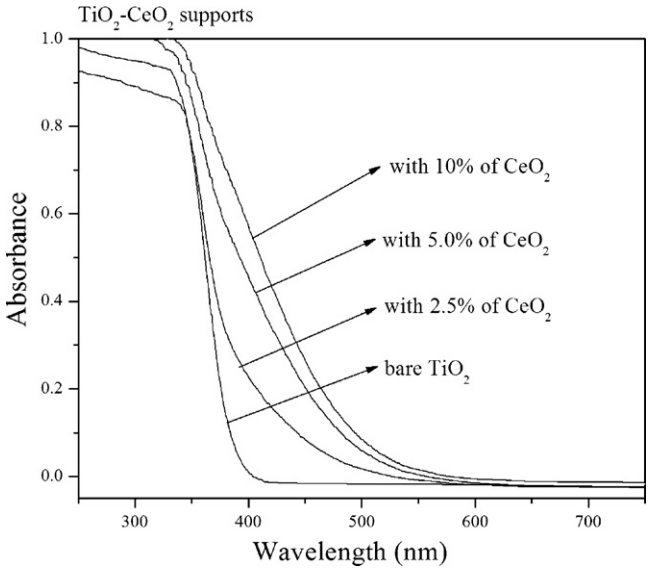

Fig. 1. UV–vis spectra for the TiO_2–CeO_2 supports.

To verify that we are in the presence of a photocatalytic process a dark test in the presence of catalysts but without UV irradiation was made and any reaction took place after 2 h in the 2,4-D solution.

3. Results and discussion

3.1. Textural and structural properties

The calculated specific surface area and the mean pore size diameter for the various TiO_2 and TiO_2–CeO_2 supports were reported in Table 1. In comparing with the bare TiO_2 solid, the specific surface area increases from 64 to 71–137 m^2/g for the TiO_2–CeO_2 samples. Large specific surface areas were obtained on the TiO_2–CeO_2 mixed oxides they increase from 64 to 71–137 m^2/g for the TiO_2 and TiO_2–CeO_2 samples respectively. The cerium effect on the specific surface area of the TiO_2–CeO_2 could be due to a modification by the cerium nitrate on the hydrolysis–condensation reactions rates of the titanium alkoxide [19–21].

In a recent paper it has been reported that for the TiO_2–CeO_2 samples only tiania anatase phase was identified by XDR, reflections identifying cerium oxide and gold particles are not observed even in the sample containing 10 wt.% CeO_2 suggesting that cerium oxides and gold are highly dispersed on the titania surface [15]. On the other hand, the study of the samples by XPS showed that the binding energy (BE) for $Au4f_{7/2}$ core level [22] on the Au/TiO_2–CeO_2 catalysts indicates that Au is present as Au^0 83.8–84.0 eV; and as oxidized gold Au^+ 85.6 eV in proportions which are comprised between 74 and 87% of reduced gold, Au^0. For cerium the $Ce3d_{5/2}$ level binding energy showed the presence of Ce^{3+}/Ce^{4+} (BE 881.9–886.2 eV) and Ce^{4+} (BE 916.15 eV) in proportions Ce^{3+}:Ce^{4+} of 49:51 and 60:40 for the catalysts containing 2.5 and 10.0 wt.% of cerium oxide respectively [15].

3.2. Photophysical properties-UV–vis absorption spectra

The band gap energy (E_g) of the samples was estimated from the UV absorption spectra (Fig. 1) taking into account that:

$$\alpha(E) = (E - E_g)^{m/2}$$

where $\alpha(E)$ is the absorption coefficient for a photon of energy *E* and $m = 1$ for an indirect transition between bands [23].

Table 1
Specific surface area, mean pore size, energy band gap and Au particle size for the Au/TiO_2–CeO_2 catalysts.

Catalyst	Pore size (Å)	Surface area ($m^2\ g^{-1}$)	λ (nm)	E_g (eV)	TEM Au (nm)
Au/TiO_2	33	64	388	3.14	8.1
Au/TiO_2–CeO_2-2.5%	53	71	403	3.00	4.4
Au/TiO_2–CeO_2-5.0%	58	117	491	2.52	3.8
Au/TiO_2-CeO_2–10%	68	137	502	2.47	3.4

λ: wavelength; E_g: band gap energy.

The band gap energies calculated by a linear fit of the slope to the abscissa are reported in Table 1; it diminishes from 3.14 eV, for the bare TiO_2, to 2.47 eV, for the TiO_2–CeO_2 (at 10 wt.%) sample. It is evident that cerium oxide modifies the bulk semiconductor properties of TiO_2. The shift of the E_g band gap to a lower energy can be attributed to the incorporation of Ce^{4+} cations, which substitute some Ti^{4+} cations.

On the other hand, the diffuse adsorption spectra of the Au/TiO_2–CeO_2 photocatalysts it appears ca. of 560 nm a broad absorption band assigned to the gold plasmon surface resonance. Kamat and Dawson [24] reports that the surface plasmon resonance of metallic nanoparticles is sensitive to the particle size, load and surrounding environment. In Fig. 2 it can be seen that the surface plasmon resonance maximum is around 625 nm for the Au/TiO_2–CeO_2-10 and Au/TiO_2–CeO_2-5.0 photocatalysts with a Au particle size of 3.40 and 3.80 nm respectively and around 600 nm for the Au/TiO_2–CeO_2-2.5 and Au/TiO_2 catalysts with Au particle size of 4.4 and 8.1 nm respectively. Thus, a particle size effect in the Au surface plasmon resonance can be observed.

3.3. Transmission electron microscopy (TEM)

The gold particle size obtained from the Z contrast images for the various photocatalysts is reported in Table 1, more than 200 gold nanoparticles supported on the TiO_2–CeO_2 catalysts were counted and measured. In Fig. 3 the gold particles can be observed as small white spots. Gold nanoparticles were found from 8.1 to 3.4 nm for Au/TiO_2 and Au/TiO_2–CeO_2-10 respectively. The small particle size obtained on the TiO_2–CeO_2 support could be due to the high specific surface area obtained in these supports (Table 1).

3.4. Photocatalytic activity

The activities of the catalysts were evaluated in the photodegradation of 2,4-dichlorophenoxyacetic acid (2,4-D) at room temperature. The photodegradation of the substrate was followed by the UV absorption band of the 2,4-D at 282 nm. The evolution of the 2,4-D as a function of time is represent in Fig. 4. From the data of these curves, the apparent rate constant K was calculated by the Integral Method for an irreversible monomolecular first order reaction [25]:

$$-r_A = -\frac{dC_A}{dt} = KC_A$$

If the batch reactor works at constant density, then:

$$\ln\left[\frac{C_A}{C_{Ao}}\right] = -kt$$

where C_A is the concentration at time t and C_{Ao} is the initial concentration.

An acceptable linearity was obtained by applying the first order kinetic equation (Fig. 5). The values calculated from selected slopes are reported in Table 2. The highest rate constant was obtained for the catalyst with 10 wt.% CeO_2 ($k = 0.0765\ s^{-1}$) to which corresponds the small gold particle size.

A representation of the gold particle size and kinetic constant as a function of the cerium oxide content is presented in Fig. 6, where it can be seen that the highest kinetic constant corresponds to the catalysts showing the lowest gold particle size (3.4 nm). In the same way the gold particle size and total organic carbon (TOC) as a function of the cerium oxide is presented in Fig. 7, the highest TOC abatement corresponds to the samples with 5.0% of cerium oxide and gold nanoparticles of 4.2 nm ($k = 0.06\ s^{-1}$). It must be expected that in samples with the small particle size, the photocatalytic activity must be more efficient due to the large contact between the gold particles and the substrate. The results in Table 2, showed that the gold particle size plays an important role in the photodegradation rate and specially in the total mineralization of 2,4-D. Thus, the better correlation for the 2,4-D photodegradation was obtained when the gold particle size was related to the total organic carbon (TOC%) eliminated in the irradiated solution.

On the other hand the stability of the catalysts were evaluated by measuring the initial activity after 4 cycles of reaction. The results are presented in Fig. 8, where it can be seen a high stability of the catalysts since the loss in activity after 4 cycles of reaction under UV irradiation is around 12%. Additionally ICP analysis of the solution after photodegradation was made in order to discard the probably gold or CeO_2 leaching during the photocatalytic reaction. In the solution after reaction the analysis report <5 ppb for Au and 90 ppb for Ce.

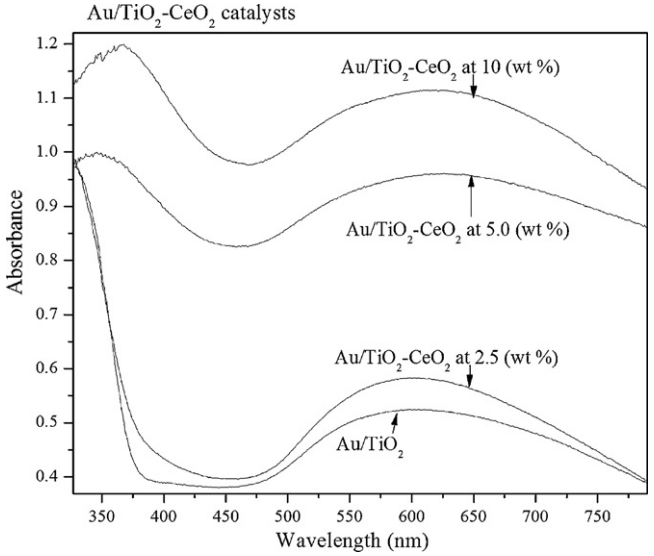

Fig. 2. UV–vis spectra for the Au/TiO_2–CeO_2 catalysts.

Table 2
Photoactivity for the 2,4-D on Au/TiO_2–CeO_2 catalysts.

Catalysts	K (s^{-1})	Convesion[a] (%)	TOC[a] (%)
Photolysis	0.0020	34.00	–
Au/TiO_2	0.0034	78.23	61.0
Au/TiO_2–CeO_2-2.5%	0.0700	99.00	82.2
Au/TiO_2–CeO_2-5.0%	0.0600	98.50	88.0
Au/TiO_2–CeO_2-10%	0.0765	99.00	81.6

K: kinetic constant; TOC: total organic carbon.
[a] After 3 h of reaction.

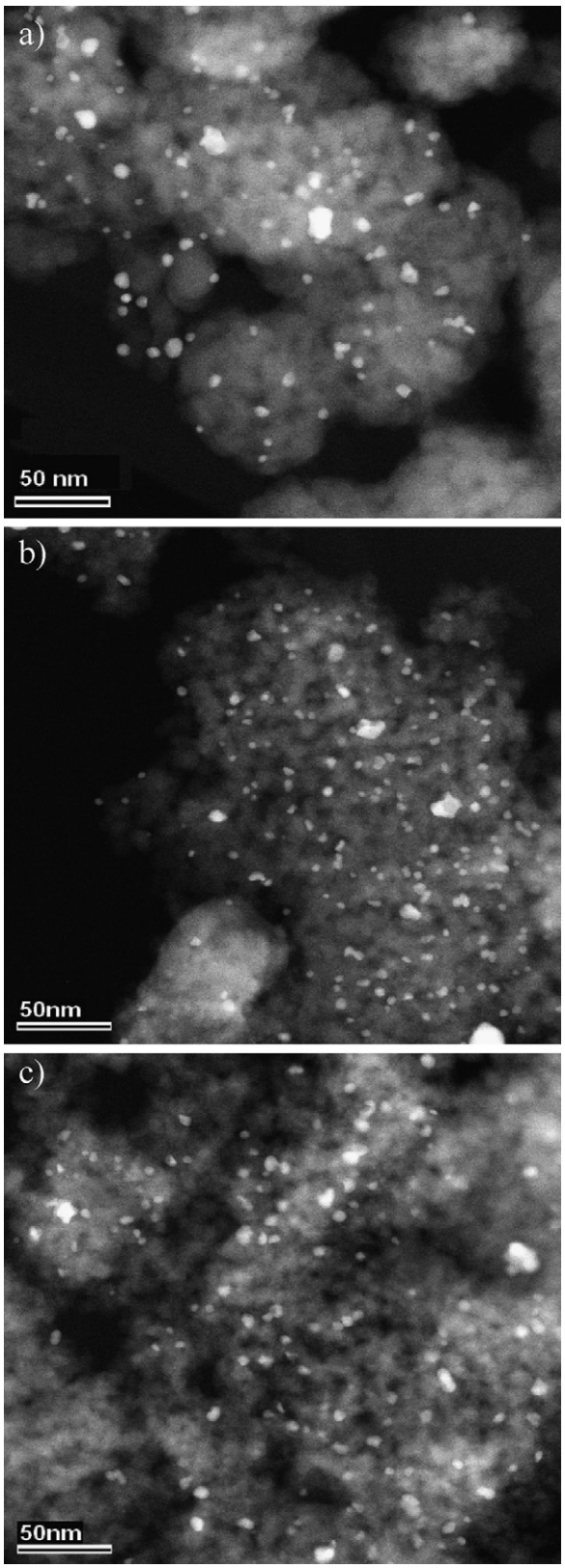

Fig. 3. HAADF image for: (a) Au/TiO_2, (b) Au/TiO_2–CeO_2-2.5 and (c) Au/TiO_2–CeO_2-10.

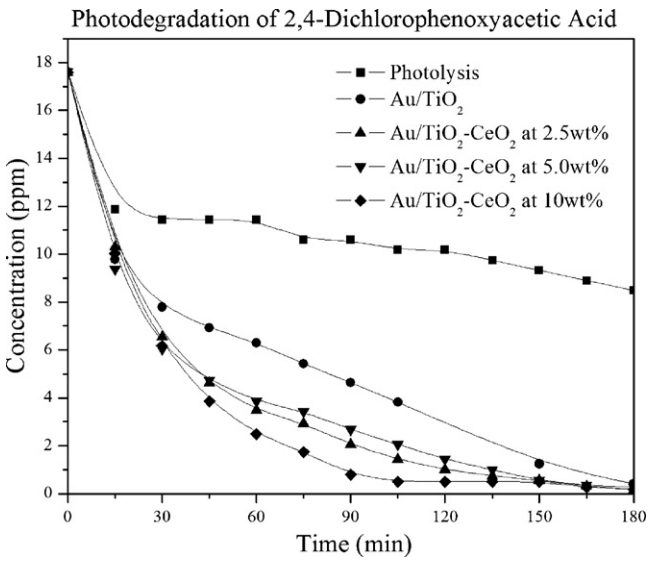

Fig. 4. Photodegradation of the 2,4-D on the Au/TiO_2–CeO_2 catalysts as a function of time.

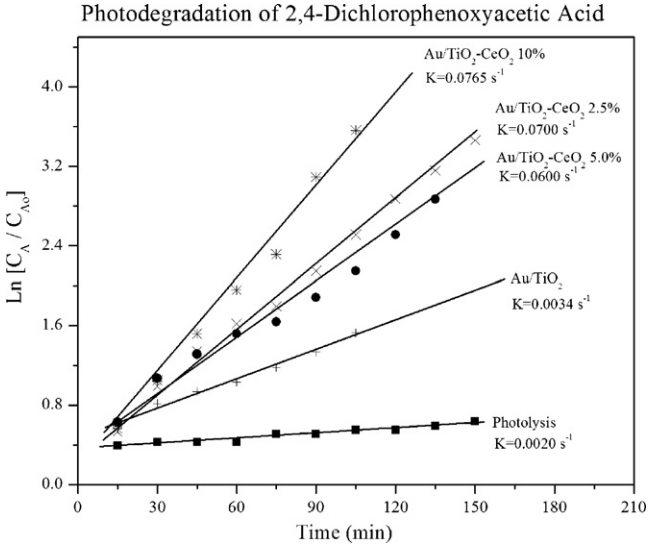

Fig. 5. Kinetic constant for the 2,4-D decomposition on the Au/TiO_2–CeO_2 catalysts.

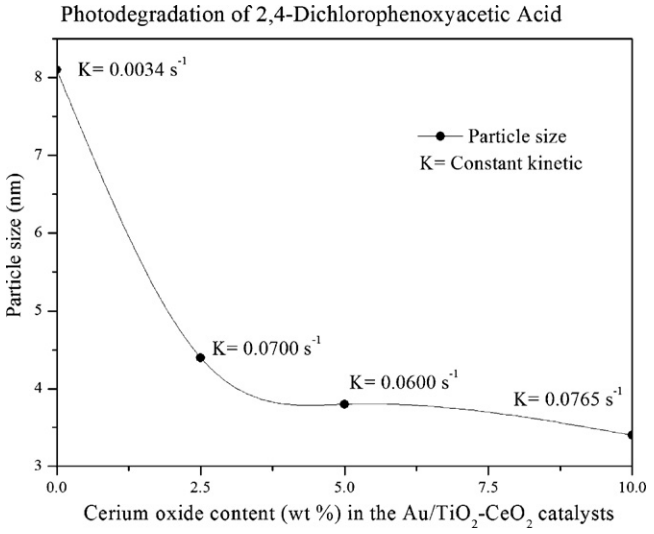

Fig. 6. Gold particle size and kinetic constant as a function of the cerium oxide content on the Au/TiO_2–CeO_2 catalysts.

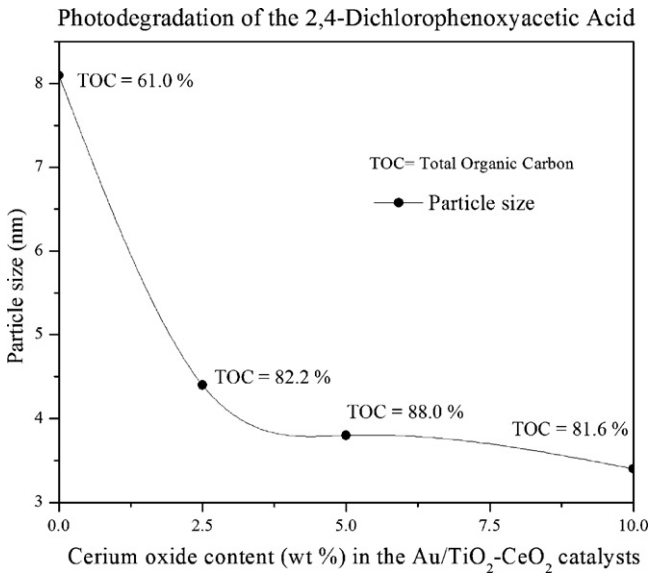

Fig. 7. Gold particle size and TOC as a function of the cerium oxide content on the Au/TiO_2–CeO_2 catalysts.

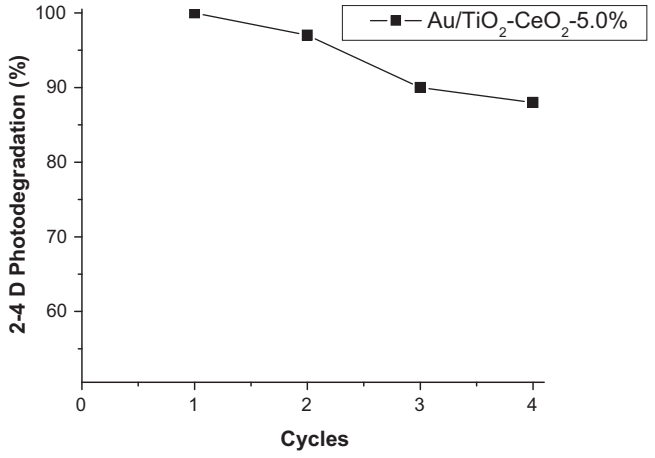

Fig. 8. Initial conversion for the 2,4-D photodegradation as a function of the number of cycles under irradiation.

In a recent paper it has been reported that for the total photodegradation of 30 ppm of 2,4-D with UV light source on the TiO_2–CeO_2 mixed oxides more than 4 h were required [7]. For comparative results in Table 3 the rate constant for the TiO_2–CeO_2 mixed oxides is reported. It can be seen that the titania–ceria oxides are an order of magnitude less active than the Au/TiO_2-CeO_2 catalysts.

As mentioned above XPS studies of the initial samples showed the presence of the redox couple Ce^{3+}/Ce^{4+} pair in the tiania-ceria photocatalysts and hence the oxygen exchange properties of cerium oxide enhanced the oxidative properties on the TiO_2–CeO_2

Table 3
Photoactivity for the 2,4-D decomposition on TiO_2–CeO_2 supports.

Substrate	K (s^{-1})	(%) Conversion after 4 h
Photolysis	0.0020	34 (3 h)
TiO_2	0.0036	60
TiO_2–CeO_2-2.5%	0.0030	74
TiO_2–CeO_2-5.0%	0.0044	87
TiO_2–CeO_2-10%	0.0040	68

K = kinetic constant.

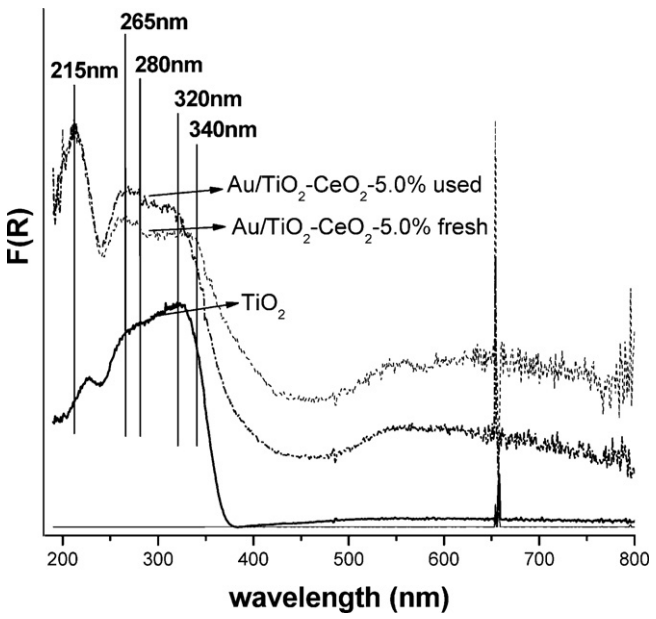

Fig. 9. UV–vis absorption spectra for TiO_2 and Au/TiO_2–CeO_2-5.0% photocatalysts fresh and used.

photocatalysts. To speak for a true catalytic effect of cerium oxide as oxidizing agent the Ce^{3+}/Ce^{4+} pair must be found in the initial and used photocatalysts. To prove that both oxidation states of cerium oxides are present in the initial and used catalysts diffuse reflectance spectroscopy (DRS–UV–vis) studies were made on both photocatalysts in the UV 200–400 nm region. The identification of cerium oxide coordination by UV–vis has been reported by Bensalem et al. [26] on CeO_2–SiO_2 solids; absorption bands at 265 and 280 nm were observed and assigned to LC (low coordination) surface Ce^{3+}–O^{2-} and to LC surface Ce^{4+}–O^{2-} oxygen transfer bands respectively. On the other hand on CeO_2–ZrO_2 mixed oxides the Ce^{3+} and Ce^{4+} charge transfer bands were localized at 250 and 297 nm respectively [27]. Thus the resolution and shift of the LC oxygen charge bands for cerium oxide depends on the environment in which cerium oxide is placed. In Fig. 9 the absorption spectra for the fresh and used photocatalysts are almost identical, a broad band in the 265–280 nm regions can be assigned to the oxygen charge transfer bands for the redox Ce^{3+}/Ce^{4+} pair. The low resolution of the spectra can be due to the presence of titania which spectrum showed also absorbance in this region. To resolve the presence of the redox Ce^{3+}/Ce^{4+} pair we put our attention to the 215 and 320–340 nm bands. They are assigned to $f \rightarrow d$ transitions of Ce^{3+} species and interband transitions in CeO_2 [26,27]. Thus the analogous spectra obtained on the fresh and used Au/TiO_2–CeO_2 photocatalysts showed real oxidizing role of the redox Ce^{3+}/Ce^{4+} pair.

The high efficiency of the combined Au and TiO_2–CeO_2 supports forming the Au/TiO_2–CeO_2 photocatalysts of the present work suggest the presence of a synergetic effect where gold plays the role of tramp of generated electrons retarding the re-combination electron–hole produced by the irradiated photons and on the other hand, the cerium oxide plays the role of important oxidizing material.

4. Conclusions

In the present work it is reported that high specific surface areas (71–137 m^2/g) can be obtained by preparing TiO_2–CeO_2 supports by the sol–gel method. It is showed that the use of the deposition–precipitation with urea method forms nanoparticles

with a size between 8.1 and 3.4 nm in depending of the CeO_2 content in the support. A cerium oxide red shift in the energy band gap was observed in the Au/TO_2–CeO_2 photocatalysts. It is proposed that the high activity showed by the Au/TO_2–CeO_2 photocatalysts can be due to a synergetic effect where gold plays the role of electrons tramp and the cerium oxide the role of oxidizing agent.

Acknowledgement

C.Guzmán thanks to CONACYT for the scholarship.

References

[1] www.epa.gov.
[2] A. Mantilla, F. Tzompantzi, J.L. Fernández, J.A.I. Díaz Góngora, G. Mendoza, R. Gómez, Catal. Today 148 (2009) 119.
[3] V. Rodríguez-González, A. Moreno-Rodríguez, M. May, F. Tzompantzi, R. Gómez, J. Photochem. Photobiol. A: Chem. 193 (2008) 266.
[4] M. Alvarez, T. López, J.A. Odriozola, M.A. Centeno, M.I. Domínguez, M. Montes, P. Quintana, D.H. Aguilar, R.D. González, Appl. Catal. B: Environ. 73 (2007) 34.
[5] S. Horikoshi, H. Hidaka, N. Serpone, J. Photochem. Photobiol. A: Chem. 159 (2003) 289.
[6] C.Y. Kwan, W. Chu, Water Res. 37 (2003) 4405.
[7] F. Galindo, R. Gómez, M. Aguilar, J. Mol. Catal. A: Chem. 281 (2008) 119.
[8] Z. Du, C. Feng, Q. Li, Y. Zhao, X. Tai, Colloids Surf. A: Physicochem. Eng. Aspects 315 (2008) 254.
[9] J. Li, Suyoulema, W. Wang, Sarina, Solid State Sci. 11 (2009) 2037.
[10] J. Li, D. Shieh, D. Li, C. Ho, S. Yang, J. Lin, Appl. Surf. Sci. 254 (2008) 4655.
[11] A. Politano, G. Chiarello, Gold Bull. 42 (2009) 195.
[12] M. Law, L.E. Greene, R. Johnson, R. Saykally, P. Yang, Nat. Mater. 4 (2005) 455.
[13] B. Tian, X. Zheng, T.J. Kempa, Y. Fang, N. Yu, G. Yu, J. Huang, C.M. Lieber, Nature 449 (2007) 885.
[14] H. Goto, K. Nosaki, K. Tomioka, S. Hara, K. Hiruma, J. Motohisa, T. Fukui, Appl. Phys. Express 2 (2009) 35004.
[15] C. Guzmán, G. Del Angel, R. Gómez, F. Galindo, R. Zanella, G. Torres, C. Angeles-Chavez, J.L.G. Fierro, J. Nano. Res. 5 (2009) 13.
[16] R. Zanella, S. Giorgio, S. Chae-Ho, C.R. Henry, C. Louis, J. Catal. 222 (2004) 357.
[17] M. Haruta, J. Catal. 36 (1997) 153.
[18] S. Lowell, J.E. Shields, M.A. Thomas, M. Thommes, Characterization of Porous Solids and Powders: Surface Area, Pore Size and Density, first ed., Kluwer Academic Publishers, Netherlands, 2004, pp. 18–43.
[19] T. Lopez, F. Rojas, R. Alexander-Katz, F. Galindo, A. Balankin, A. Buljan, J. Solid State Chem. 177 (2004) 1873.
[20] X. Bokhimi, R. Zanella, J. Phys. Chem. C 111 (2007) 2525.
[21] F. Galindo-Hernández, R. Gómez, G. Del Ángel, C. Guzmán, J. Ceram Process Res. 9 (2008) 616.
[22] G.E. Mulillenberg, Handbook of X-Ray Photoelectron Spectroscopy, Perkin-Elmer Corporation, Phisycal Electronics division, USA, 1978.
[23] M. Anpo, Pure Appl. Chem. 72 (2000) 1265.
[24] P.A. Dawson, P.V. Kamat, J. Phys. Chem. B 105 (2001) 960.
[25] O. Levenspiel, Chemical Reaction Engineering, John Wiley & Sons, Inc., New York, 1990, p. 50.
[26] A. Bensalem, J.C. Muller, F. Bozon-Verduraz, J. Chem. Soc. Faraday Trans. 88 (1992) 153.
[27] G. Ranga Rao, H. Ranjan Sahu, Proc. Indian Acad. Sci. (Chem. Sci.) 113 (2001) 651.